Environmental Science & Technology

pubs.acs.org/est

Article

Hitchhiking into the Deep: How Microplastic Particles are Exported through the Biological Carbon Pump in the North Atlantic Ocean

Luisa Galgani,* Isabel Goßmann, Barbara Scholz-Böttcher, Xiangtao Jiang, Zhanfei Liu, Lindsay Scheidemann, Cathleen Schlundt, and Anja Engel

Cite This: https://doi.org/10.1021/acs.est.2c04712

Read Online

ACCESS | Metrics & More | Article Recommendations | Supporting Information

ABSTRACT: Understanding residence times of plastic in the ocean is a major knowledge gap in plastic pollution studies. Observations report a large mismatch between plastic load estimates from worldwide production and disposal and actual plastics floating at the sea surface. Surveys of the water column, from the surface to the deep sea, are rare. Most recent work, therefore, addressed the "missing plastic" question using modeling or laboratory approaches proposing biofouling and degradation as the main removal processes in the ocean. Through organic matrices, plastic can affect the biogeochemical and microbial cycling of carbon and nutrients. For the first time, we provide *in situ* measured vertical fluxes of microplastics deploying drifting sediment traps in the North Atlantic Gyre from 50 m down to 600 m depth, showing that through biogenic polymers plastic can be embedded into rapidly sinking particles also known as marine snow. We furthermore show that the carbon contained in plastic can represent up to 3.8% of the total downward flux of particulate organic carbon. Our results shed light on important pathways regulating the transport of microplastics in marine systems and on potential interactions with the marine carbon cycle, suggesting microplastic removal through the "biological plastic pump".

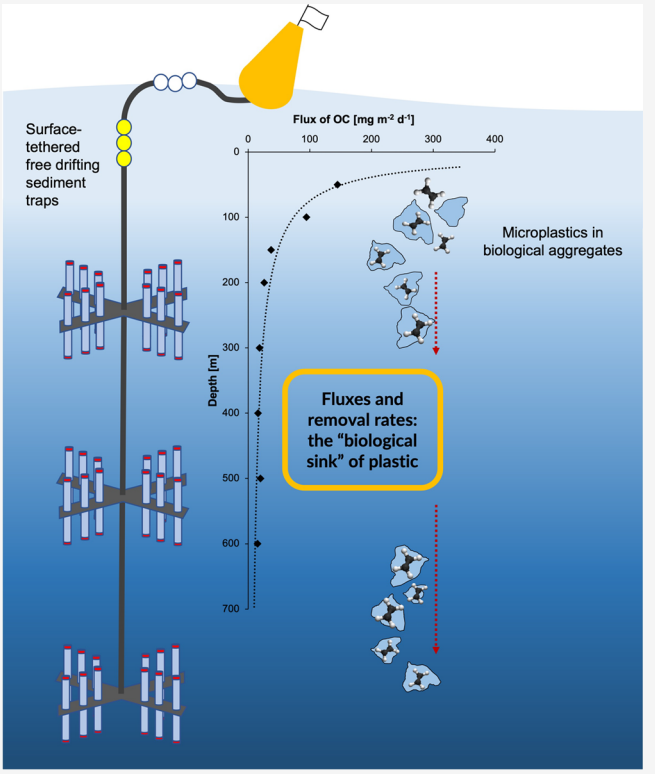

KEYWORDS: *microplastics, sediment trap, sinking marine aggregates, marine snow, microplastic export fluxes, biological plastic sink*

INTRODUCTION

It is not surprising that plastic has found its way to the most remote and pristine locations,[1−3] becoming an ubiquitous and pervasive element of marine environments, biota, inland waters, soils,[4] and air[5,6] and a planetary boundary threat.[7] A recent study suggested that the beginning and end processes of the plastic life cycle (industrial production and incineration) can release high amount of chloride, which strongly contributes to atmospheric aerosol growth and concentration.[8] The marine environment, through riverine input of mismanaged plastic waste[9,10] and underestimated sources emerging from ship coatings,[11−13] is the ultimate collector of this relatively new kind of pollution, now a common component of seawater; plastic is so omnipresent to be considered having its own biogeochemical cycle.[14] An estimated amount of plastic presumably present in the ocean in 2020 is as high as 150 million metric tons (MT).[15] For an average 80% carbon content in plastic (by weight), we would have 120 million MT of plastic-bound carbon in the ocean today. The ocean is a massive carbon reservoir that naturally holds about 38,400 Pg C;[16] in this respect, plastic-bound carbon represents only a small contribution to the global marine carbon budget (0.0003%). However, this small contribution can potentially

Received: June 30, 2022
Revised: September 28, 2022
Accepted: September 29, 2022

imply a significant impact on carbon cycling: plastic leachates as dissolved organic carbon are rapidly metabolized by microorganisms,[17] and at the same time, microplastics are substrates for high microbial activity and organic matter turnover.[18−20] Particle-attached microbial communities might greatly differ from the free-living microbes of the surrounding seawater, and organisms found abundant on natural marine aggregates identified in the class *Gammaproteobacteria* (*Pseudomonadota* phylum, including *Vibrio* spp.), in the genus *Cytophaga* (phylum *Bacteroidetes*), and in the phylum *Cyanobacteria* are also common on plastic debris.[21−23]

A recent model proposed that in marine areas of high plastic and nutrient concentration, grazing pressure on phytoplankton is reduced: this leads to initial high rates of biological production that in the long term may regionally compromise the oxygen inventory through accelerated biomass degradation.[24]

Microplastics interact with suspended inorganic and organic components of seawater, including extracellular polymeric substances (EPS), mucilaginous material exuded by microorganisms that helps forming plastic agglomerates in seawater;[25] microplastics <1 mm in size are incorporated into marine aggregates,[26] often referred to as marine snow, but particles even smaller (∼30−100 μm) can support the formation of marine biogenic polymer gels.[20,27] Such gels in their polysaccharidic (transparent exopolymer particles, TEP) and proteinaceous (Coomassie stainable particles, CSP) composition find their origin in dissolved polymeric precursors from biological production and degradation processes. Due to their high stickiness, gel-like particles accelerate particle coagulation rates and play a pivotal role in the vertical transport of organic matter and carbon.[28,29] Similarly, these gel-like particles can interact with microplastics, regulating their buoyancy and bioavailability in the oceans.[27,30] Marine snow particles are an essential component of the biological carbon pump, the fundamental oceanic process encompassing all mechanisms of atmospheric carbon sequestration (as dissolved CO_2), its incorporation into particulate and dissolved organic matter through photosynthesis, and its vertical transport to the ocean's interior. In its descent, part of the organic matter is remineralized through the microbial loop or ingested by macro-organisms. At the same time, other fractions make their way to marine sediments contributing to the millennia oceanic carbon storage.[31] By interacting with marine snow and marine gel particles, plastic particles not only benefit from the biological carbon pump as a vertical downward transport process but simultaneously interfere with the whole mechanism of carbon sequestration, turnover, and storage.[32,33]

The North Atlantic Gyre is one of the largest convergence zones for surface plastic debris[34] and first published observations date back to the early 70s.[35] Continuous plankton tow data for the North-East Atlantic Ocean report a constant increase of surface ocean plastic from the mid-1950s to 2016 recorded as co-entanglement and faults on ships-of-opportunity.[36] Depth-resolved observations show that concentrations of polyethylene, polypropylene, and polystyrene microplastics are high in the upper 270 m across all latitudes from the North to the South Atlantic.[37] Moreover, plastic has been present in sediments and deep-sea invertebrates of the Rockall Trough (>2000 m, North-East Atlantic) for the past 50 years at least.[38,39] Aggregation with organic matter and the subsequent vertical transport within rapidly sinking marine snow and fecal pellets are suggested as important mechanisms of microplastic removal from the surface ocean.[40] These processes may determine microplastic accumulation in the deep North Atlantic and Pacific basins.[40] However, most of the plastic assumed reaching the ocean escapes current monitoring surveys.[41,42] Despite decades of available data for global ocean surface plastics[34,41,43] and more recent models on potential removal processes,[40,44] observations of the water column are still scarce.[45] Yet, it may represent one of the largest reservoirs of marine microplastics as suggested by mass measurements in the German Bight.[11,37] Mesopelagic plastic concentration and fluxes in high plastic accumulation zones such as the North Atlantic Gyre are fundamental information to explore vertical transport and particles' fate, while suggesting mitigation actions for marine regions not yet as much affected by plastic pollution.

Here, we present the first data on microplastics vertical export in the North Atlantic Gyre based on two deployments of surface-tethered drifting sediment traps with eight depth intervals from 50 to 600 m (Figures S1 and S2, Table S1). The study was conducted during the POS536 cruise "DIPLANOAGAP: Distribution of Plastics in the North Atlantic Garbage Patch" (August 17−September 12, 2019). Surface-tethered drifting sediment traps capture sinking particles in the upper ocean to study the biological control over the removal of abiogenic particles from the surface.[46−49] We applied this approach to track fluxes and the interaction with sinking organic matter driving microplastic removal from the surface in the large accumulation zone of the North Atlantic, and we quantified the carbon contained in plastic (plastic-C) to estimate its contribution to particulate organic carbon (POC) fluxes. Moreover, we gathered microplastic debris (1 mm) in 300 m depth to visualize microscopically the spatial arrangement and bacterial composition of biofilms growing on the debris. To the best of our knowledge, this work represents the first observation of mesopelagic microplastic fluxes in the North Atlantic Gyre linked to biological sinking material establishing a direct connection to the missing plastics in the ocean.

MATERIALS AND METHODS

Traps Deployment. During POS536 cruise, free-floating surface-tethered traps (Figure S1) were deployed to collect passively sinking particulate matter and plastic particles, with a setup as described in Engel et al. (2017)[46] and Knauer et al. (1979).[48] The material collected was pre-screened (500 μm) to remove zooplankton and visible plastics for later separate identification. Eight free-floating PVC sediment arrays were mounted on a line to collect sinking material at 50, 100, 150, 200, 300, 400, 500, and 600 m. Each array contained twelve individual collectors (particle interceptor trap, PIT)[48] of which two were blank controls (Figure S2). Each PIT [a 2 L plexiglass-poly(methyl methacrylate) (PMMA)-tube] was filled with ∼1.5 L of filtered seawater (0.2 μm) collected from 300 m depth a few days before the deployment and 500 mL of pre-filtered (0.2 μm) brine solution, prepared with 50 g NaCl per L of seawater. The brine solution was pumped to the bottom of each PIT and below the pre-filled seawater with an acid-washed tube and a peristaltic pump. All PITs were immediately covered and stored upright until deployment, which was done within a maximum of 2 h from the solutions' preparation. The density gradient allows sinking particles to enter the PITs preventing their escape and is necessary to prevent flushing when recovering the traps. The density stratification is maintained by underwater pressure when lowering the traps, and previous studies have shown (by the use of specific dyes) that such density gradient is maintained at depth.[48] In our experiment, we visually inspected all PITs before

https://doi.org/10.1021/acs.est.2c04712
Environ. Sci. Technol. XXXX, XXX, XXX−XXX

Table 1. Masses in the PITs ($\mu g\ L^{-1}$) of Individual Cluster of Polymer Types Identified by Py-GC/MS and Total Mass of Plastic from Deployment#2[a]

depth	C-PE	C-PP	C-PET	C-PS	C-PVC	C-PC	C-PMMA	C-PA6	C-MDI-PUR	total mass $\mu g\ L^{-1}$
50 m	+	7.3	5.4	0.1	+	0.2	3.0	n.d.	n.d.	16.0
100 m	n.d.	20.5	13.0	0.1	+	0.8	10.4	n.d.	n.d.	44.9
150 m	5.9	0.2	3.8	+	+	+	25.2	n.d.	n.d.	35.1
200 m	+	0.2	7.7	0.3	+	*	1.5	n.d.	n.d.	9.7
300 m	0.9	+	1.6	+	+	*	+	n.d.	*	2.6
400 m	n.d.	14.8	1.9	+	+	+	0.7	n.d.	n.d.	17.4
500 m	+	+	*	+	+	*	+	n.d.	*	0.0
600 m	+	2.0	0.6	+	+	0.6	0.5	n.d.	n.d.	3.6
total mass										129.3
% over the total amount	**5.2**	**34.9**	**27.3**	**0.5**	**0.0**	**1.2**	**30.9**	**0.0**	**0.0**	100
average density g cm^{-3}	0.97	0.86	1.33	1.05	(1.39)	1.17	1.16	(1.13)	(1.23)	

[a]+ indicates negative values after blank subtraction; * indicates traces, not quantifiable amount; n.d. not detected.

deployment and after recovery to make sure that the density gradient was maintained and it was found intact or a few centimeters above. The size of each PIT led to an aspect ratio of 7.5 as described in Engel et al.[46] and together with the top baffle, the configuration helped reducing drag-induced movements within the trap.[50]

Each PIT was closed at the bottom with a low-density polyethylene lid. Ten traps per array had a top plexiglass baffle to restrain the flux of larger material (>1 cm). The two blank PITs were covered with the low-density polyethylene lid and did not collect any material.

Sediment traps were deployed twice (Table S1) and remained free-floating for 5 days allowing the collection of enough sinking material. This system has been previously tested in several cruises.[46,51] Each array is hooked to a main line marked for specific depths, attached to a ground weight of 70 kg and to different floats and a yellow buoy at the top (Figure S2) which carries two GPS beacons: an Argos and an iridium system and a flashlight for tracking and recovery. Sediment trap#1 slowly drifted toward North-West and was recovered at approximately 15 nautical miles from the deployment location, whereas sediment trap#2 drifted North-East and was recovered at 13 nautical miles from the deployment location.

After recovery, all PITs were treated according to Engel et al. (2017)[46] without the addition of formalin. Seawater was pumped out of each PIT until reaching 3 cm above the density gradient. The remaining brine solution was the actual sample, and successively, aliquots of samples were immediately filtered under low pressure (<200 mbar); filters were stored frozen (−20 °C) or dried until analyses.

Transfer efficiencies for particulate components were calculated as the ratio of fluxes at 600 m to those at 100 m as in Engel et al. (2017).[46] Data on particulate matter fluxes, pyrolysis gas chromatography coupled with mass spectrometry (Py-GC/MS), and Fourier transform infrared (FT-IR) spectroscopy of plastic polymer mass were fitted to the normalized power function $F_Z = F_{100}(z/100)^b$ with F_{100} as the flux at a depth (z) of 100 m and b attenuation coefficients indicating that the more negative is b, the higher is the flux attenuation.[52]

Biogenic Parameters: Total Particulate Mass, Chlorophyll *a*, Marine Gels (TEP and CSP), POC, and Particulate Nitrogen. Total particulate mass was analyzed in triplicate and aliquots were filtered onto pre-weighed 0.4 μm polycarbonate filters. Filters were rinsed twice with Milli-Q water, dried at 60 °C for 4 h, and stored until weight measurement on a Mettler Toledo XP2U microbalance.

Chlorophyll *a* was determined in triplicate and aliquots filtered onto combusted GF/F filters were kept frozen (−20 °C) until analysis. Samples were analyzed after extraction with 10 mL of acetone (90%) on a Turner fluorometer after Welschmeyer (1994).[53] Calibration of the instrument was conducted with a spinach extract standard (Sigma-Aldrich).

TEP and CSP were determined in quadruplet by microscopy after Engel (2009).[54] Samples were stored at −20 °C until microscopy analysis with a light microscope (Zeiss Axio Scope A.1) connected to a camera (AxioCam MRc). Filters were screened at 200× magnification. Thirty pictures were taken randomly from each filter in two perpendicular cross sections. Image analysis software WCIF ImageJ (US National Institutes of Health) was used to semiautomatically analyze particle numbers and area. TEP carbon content (TEP-C) was estimated after Mari (1999)[55] according to the relationship

$$\text{TEP} - C = a\Sigma_i(n_i r_i^D) \quad (1)$$

with n_i being the number of TEP in the size class i and r_i the mean equivalent spherical radius of the size class. The constant $a = 0.25 \times 10^{-6}$ (μg C) and the fractal dimension of aggregates $D = 2.55$ were proposed by Mari.[55]

POC and particulate nitrogen (PN) aliquots were filtered in triplicate onto combusted (8 h at 500 °C) GF/F filters (Whatman, 25 mm) and kept frozen (−20 °C) until analysis. Filters were exposed to fuming hydrochloric acid in a fuming box overnight to remove carbonate and subsequently dried (60 °C, 12 h). For analysis, the filters were enclosed in tin cups and analyzed using a Euro EA elemental analyzer calibrated with an acetanilide standard.

Py-GC/MS. Py-GC/MS measurements, calibration, and quantification were performed as already published.[56] Py-GC/MS measurement conditions are described in Table S2. Polymers for calibration and quantification are given in Table S3. Deuterated polystyrene was used for internal standardization.[57] For the polymers, the prefix "*C*"[11,58] indicates that the polymer-specific indicator ions include the polymer itself, but also polymers related to the same monomer (e.g., copolymers and polymer-containing formulations). Further details are described in Table S4. Carbon contents were calculated based on the mass of each polymer (Table 1) and the respective carbon content within the pure polymer (Table S5).

In detail, for Py-GC/MS aliquots of 2 L (from deployment#2 only) were filtered onto stainless-steel filters (pore size 10 μm) and rinsed with hydrogen peroxide (pre-filtered 1 μm). The filter residues were filtered through a GF/F (15 mm diameter,

https://doi.org/10.1021/acs.est.2c04712
Environ. Sci. Technol. XXXX, XXX, XXX−XXX

1 μm pore size, Pall Life Sciences; pre-treated in a muffle furnace at 400 °C for 4 h). The GF/F, including the filter cake, was folded and transferred into a stainless-steel pyrolysis cup (Eco Cups 80 LF, Frontier Labs, Japan). Full procedural laboratory blanks were prepared identically for each sample set and subtracted from raw data of trap samples. More specifically, even if only pre-filtered solvents, cleaned glassware and thermally treated glass fiber filters were used for sample processing in the laboratory, small signals occur in the laboratory blanks for some polymer cluster due to the sensitivity of the Py-GC/MS. Because the same chemicals and equipment were used for these laboratory blanks as for the samples in terms of type and volumes, the signals of the laboratory blanks were subtracted from those of the sample to avoid any potential over-quantification. For this purpose, mean peak area ratios for respective trace signal of polymer clusters were also calculated for the laboratory blanks (n = 3), which were then subtracted from the peak area ratios of the samples (thus based on the raw data) before the actual quantification. This laboratory blank value subtraction was not carried out for the ship blank values because these samples were processed directly on the ship and no further additional processing in the laboratory was necessary before Py-GC/MS measurement. In fact, one blank-control PIT per depth was filtered onto GF/F filters on board. These filters were directly placed into pyrolysis cups and quantified with Py-GC/MS to determine any secondary contamination of the PIT itself. A mean value from these blank-control PITs was calculated and subtracted from the data set, to exclude contamination of the sampling device. This resulted in a reduced number of polymers finally considered in the discussion. In the case of *C*-PVC, a constant *C*-PVC background was found in the trap blanks that exceeded the levels in the samples. This was taken as an indication of systematic contamination of the samples during sampling. Accordingly, *C*-PVC was excluded from further discussion.

For deployment#1, in the absence of enough sample to be processed for Py-GC/MS, data on plastic mass as well as carbon content (μg L^{-1}) were extrapolated by a linear regression relationship (R^2 = 0.725, p = 0.007) between chlorophyll *a* (Chl *a*) and plastic mass for deployment#2 since chlorophyll *a* concentration was not significantly different between the two deployments (t-test, $p > 0.05$):

$$\text{Plastic mass } [\mu\text{g L}^{-1}] = 2.106 + (19.424 \times \text{Chl } a(\mu\text{g L}^{-1})) \quad (2)$$

FT-IR for Particles Larger than 20 μm. For FT-IR analysis, between 200 and 400 mL of pooled samples per depth and deployment were filtered in triplicate through pre-combusted GF/F filters and stored in pre-combusted glass Petri dishes. GF/F filters were pre-combusted to avoid any possible organic contamination as applied in previous studies.[59,60] Filters were scanned for microplastics for a quarter of the size or a half of the size (Table S6). The total mass flux was calculated according to the scanned areas. The FT-IR spectrophotometer (IR Tracer-100, Shimadzu, Japan) was coupled with an automatic infrared microscope (AIM-9000, Shimadzu, Japan). Possible microplastics were first located on the filters using the wide-field camera; the measurements were made in transmittance or reflectance mode using the liquid nitrogen cooled wide-band mercury cadmium telluride detector. The measurement conditions were wavelength range, 500−4,000 cm^{-1}; resolution, 8 cm^{-1}; cumulated number, 32 scans; apodization function, Sqr-triangle; and aperture size, 20 μm × 20 μm. The background noise was measured under blank filters and removed from sample background automatically. The heterogeneous surface of the GF/F filters did not affect the detection of possible microplastics in this study, given the fact that the detection limit of the FT-IR spectrophotometer was set to 20 μm, which is far larger than the lines/fibers on the filters. This detection limit also allowed a matching score above 500.

Polymers were identified by comparing the sample spectrum to a library (Table S7). The match acceptance criteria ranged from 620 to 800 score (1000 as the highest), and the highest match rate was adopted. Area, equivalent spherical diameter (ESD) or size, density, mass, and carbon content of the particles were calculated (Table S7). To determine the area and the ESD of the particles, samples were categorized in fibers and fragments. The fiber was estimated as a cylinder with length and width (radius) estimated on the microscope photo by comparison with the 25 μm proportional scale label (Table S7, ESD†). For fragments, a photo of the sample was divided into 264 × 200 pixel grids and analyzed by Pixelmator Pro software. The area was estimated by converting the grids of the sample contained based on the color differences using the 25 μm scale label (where 25 μm length equals to 16 pixel grids).

Samples for FT-IR were not meant to provide a direct comparison with Py-GC/MS data. Both approaches use different detection techniques. A direct comparison would require exactly the same processing with regard to the recorded particle sizes as well as a consistent harmonization of the data sets, which was not possible due to the given framework conditions. Both methods have advantages and disadvantages: the strength of the Py-GC/MS is mass determination of different polymers to catch the flux of plastic and its related carbon, while FT-IR give deeper insights in size or shape different plastic particle.

Biofilm Imaging Using Combinatorial Labeling and Spectral Imaging−Fluorescence *In Situ* Hybridization. Biofilm imaging was performed on one sample collected at 300 m depth, as suitable samples for this type of analysis were not retrieved at other depths. Sample preparation and microscope imaging were as described in Schlundt et al. (2019)[61] with the following modifications. We used a confocal laser scanning microscope Leica TCS SP5 II and the objective Leica HCX PL APO CS 60 × 1.4 OIL. Spectral images were acquired using simultaneous excitation with 488, 543, and 633 laser lines with laser intensities of 40, 60, and 15%, respectively, and a laser gain of 730 with an offset of −7%. Images were captured in the lambda mode by recording 26 lambda sections in the row with a bandwidth of 10 nm wavelength ranging from 500 to 730 nm. We applied a line average of 2 and the bidirectional mode. We acquired z-stacks of up to 10 μm in thickness to bring curved surfaces of the plastic samples in an even focus plane. Linear unmixing was conducted with Leica software LAS AF. We applied a nested probe set as described in Schlundt et al. (2019)[61] using seven different probes dual labeled with fluorophores. The probes Eub338-I, Eub338-II, and Eub338-III were labeled with Atto532 to target the entire domain Bacteria. The probe Alf968 labeled with Atto514 targets the class *Alphaproteobacteria*, Gam42a labeled with Cy5 targets the class *Gammaproteobacteria*, Bac1058 labeled with Atto490SL targets the phylum *Bacteroidetes*, and Rho1682 labeled with Atto565 targets the family *Rhodobacteraceae*.

Microplastic Removal Rates. Plastic particle theoretical sinking velocities were calculated using Stokes' formula for particles with a density higher than seawater[45]

https://doi.org/10.1021/acs.est.2c04712
Environ. Sci. Technol. XXXX, XXX, XXX−XXX

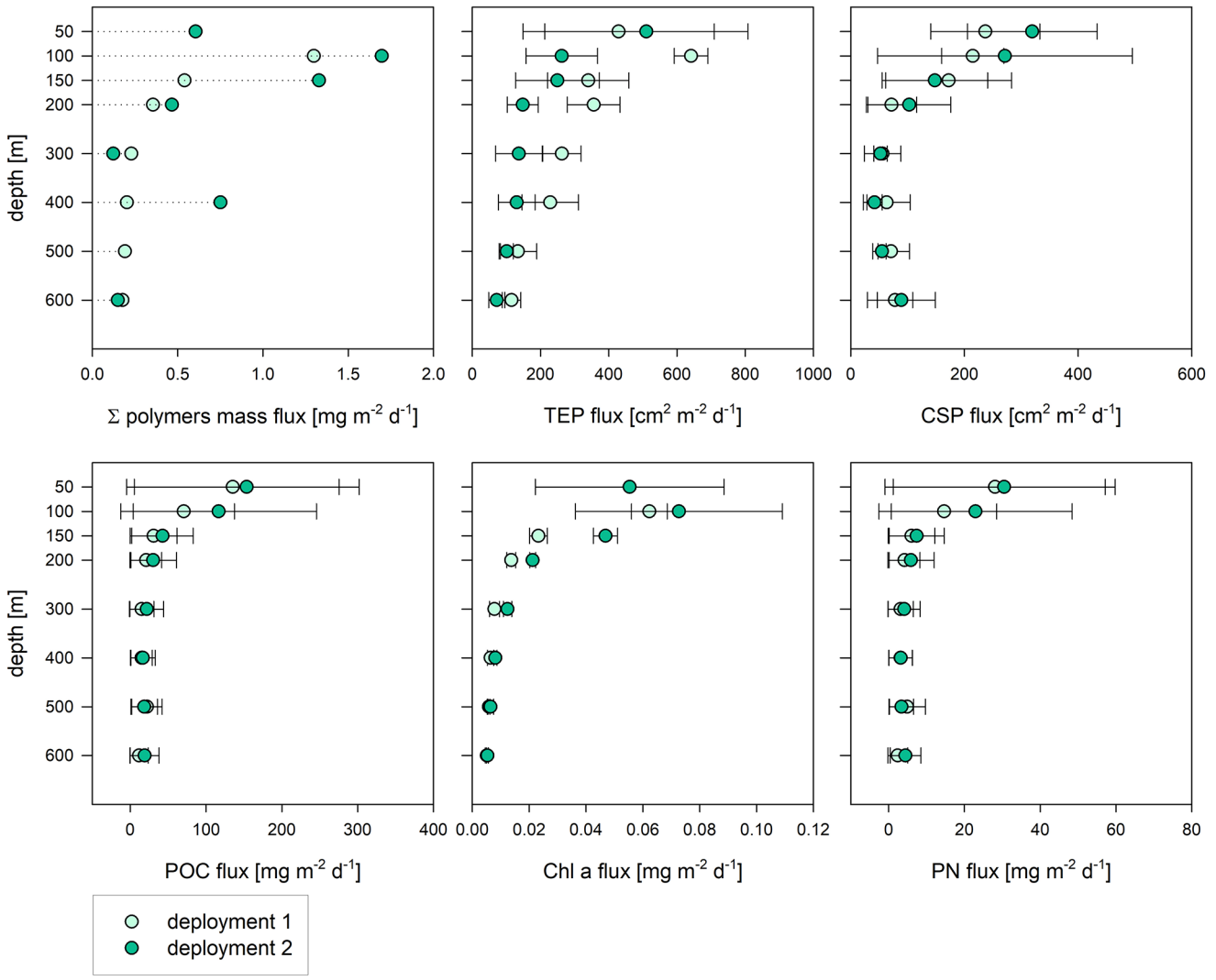

Figure 1. Fluxes of Py-GC/MS plastic polymer mass, TEP, CSP, POC, Chl *a*, and PN per each deployment. Data from deployment#1 for Py-GC/MS have been extrapolated from eq 2 (Materials and Methods).

$$v = 2(\rho_p - \rho_{sw})gR^2/9\mu \quad (3)$$

where ρ_p is the density of the particles (g cm^{-3}, Table 1), ρ_{sw} is the average density of seawater in the sampling region of the two deployments for the upper 650 m of the water column (1.028 g cm^{-3}), g is the gravitational field (m s^{-2}), R is the radius of an ESD, and μ is the dynamic viscosity of seawater ($\sim 10^{-3}$ Kg m^{-1} s^{-1}) from Ardekani and Stocker.[62]

Statistical Analysis and Graphics. Statistical analysis (linear regression, Spearman correlation analysis, and paired *t*-tests) was performed with SigmaPlot 12 (Systat Software, Inc.), Microsoft Excel 365, and Prism 8.02 (GraphPad Software, San Diego, CA, USA). Statistical significance was accepted for $p < 0.05$ (two-tailed). Figure S1 was obtained with Ocean Data View (v. 5.5.1), https://odv.awi.de. The abstract graphics was drawn with PowerPoint 365 subscription.

RESULTS

In this study, we applied two distinct analytical approaches for microplastics, Py-GC/MS and FT-IR. The minimum particle detection size for Py-GC/MS was 10 μm (stainless-steel filter pore size); with FT-IR analysis, the detection limit was set to all particles above 20 μm × 20 μm.

Polymer identification by FT-IR analysis was performed on a spectral library basis (Table S7). Py-GC/MS identified polymers later categorized in nine polymer clusters indicated by the prefix "*C*" and related to a pure basic polymer type according to Primpke et al.[58] and Dibke et al.[11] as *C*-polyethylene (*C*-PE), *C*-polypropylene (*C*-PP), *C*-polyethylene terephthalate (*C*-PET), *C*-polystyrene (*C*-PS), *C*-polyvinyl-chloride (*C*-PVC), *C*-polycarbonate (*C*-PC), *C*-polymethyl methacrylate (*C*-PMMA), *C*-polyamide-6 (*C*-PA6), and *C*-methylene diphenyl diisocyanate polyurethane (*C*-MDI-PUR) (Tables 1 and S4). Py-GC/MS was only performed on samples from deployment#2. The mass of plastic from deployment#1 was extrapolated based on chlorophyll-*a* and plastic mass data from deployment#2 (eq 2, Materials and Methods). In deployment#2, Py-GC/MS detected all polymer types with a high percentage over the total amount represented by the clusters *C*-PET, *C*-PP, and *C*-PMMA (Table 1).

Particles detected by FT-IR were fragments and fibers of a median size of 62.5 μm for 36.7% in the C-PE cluster, 3.3% in the C-PS cluster, 3.3% in the C-PA6 cluster, 43.3% of non-identified cluster, and 13.3% as copolymers (Table S7), in numbers varying between 0.2 and 5.4 particles per L from both deployments (Table S6). The converted mass of the particles

https://doi.org/10.1021/acs.est.2c04712
Environ. Sci. Technol. XXXX, XXX, XXX−XXX

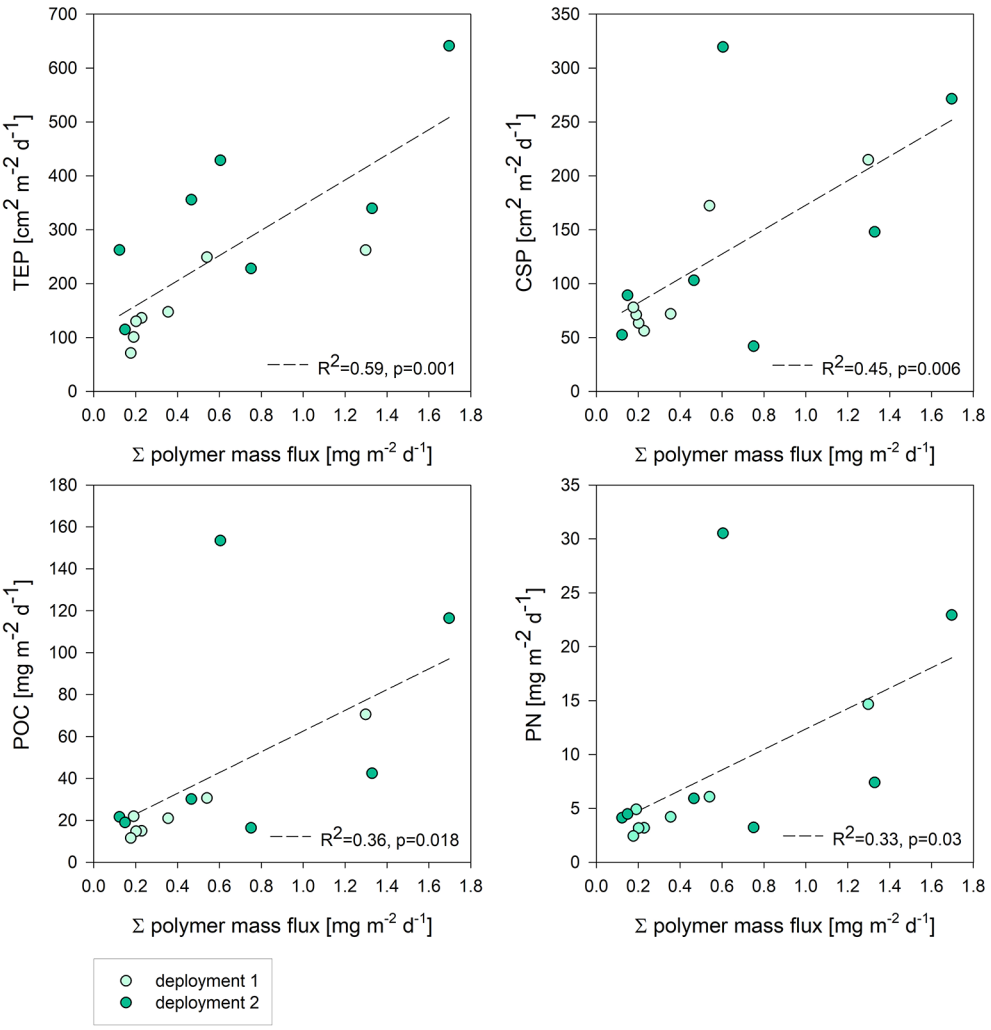

Figure 2. Export fluxes of TEP, CSP, POC, and PN in relation to polymer mass flux analyzed by Py-GC/MS for both deployments together because differences in the parameters were not significant and *in situ* conditions were quite the same. Linear regression R^2 and p values are noted in each graph. Fluxes for Py-GC/MS mass in deployment#1 have been extrapolated according to eq 2 (Materials and Methods).

represented 1.6 ± 2.6% (deployment#1) and 0.6 ± 1.5% (deployment#2) of the mass analyzed by Py-GC/MS.

For Py-GC/MS, all trap samples were subjected to lab blank correction for lab treatment. For this purpose, a peak area ratio was also calculated for the signals contained in the lab blanks and these were subtracted from the peak area ratios of the samples. This was done on a raw data basis, that is, before quantification. No correction was necessary for the trap blanks directly filtered on board and directly transferred to Py-GC/MS cups without further lab treatment (Materials and Methods, Figure S3). Subsequently, all Py-GC/MS data were corrected for the sampling device blank (trap blank) as well. This resulted in a reduced number of identified polymer clusters in traceable quantities in declining order of abundance: *C*-PP, *C*-PMMA, *C*-PET, *C*-PE, *C*-PC, and *C*-PS (Table 1). Plastic was detected at every depth (Figure 1) with the highest amounts in the upper 150 m (74.3%) and at 400 m, and this latter represented 13.4% of all plastic mass found in the deployment added up over all depths (Table 1). Trace amounts of plastic occurred at 600 m as well (2.7% of plastic mass).

The export flux of plastic polymer mass by Py-GC/MS in deployment#2 ranged between 0.12 mg (300 m) and 1.7 mg m^{-2} d^{-1} (100 m) with an average of all depths of 0.73 ± 0.59 mg $m^{-2}d^{-1}$. The depth-diminishing flux profile was fitted by a power-law relationship (Martin Curve; Materials and Methods) and compared to the flux attenuation of biogenic compounds such as TEP, CSP, POC, and PN (Figure 2). The extrapolated flux of plastic mass for deployment#1 (eq 2) ranged between 0.2 (600 m) and 1.3 mg m^{-2} d^{-1} (100 m), with an average over all depths of 0.43 ± 0.4 mg m^{-2} d^{-1}. In terms of plastic carbon flux, this equals to an average of all depths of 0.46 ± 0.43 mg m^{-2} d^{-1} (deployment#2) and 0.31 ± 0.29 mg m^{-2} d^{-1} (deployment#1), with maxima at 100 m depth for both deployments.

The plastic carbon flux (plastic-C) by Py-GC/MS contributed between 0.3 and 3.8% (deployment#2) and between 0.6 and 1.3% (deployment#1, extrapolated) to the POC flux (Figure S4) and more than TEP carbon (TEP-C), which contributed only between 0.04 and 0.12% (deployment#1) and 0.04 and 0.17% (deployment#2). We did not observe significant differences between the two deployments in the fluxes of TEP, CSP, POC, chlorophyll *a*, and PN (*t*-test, $p > 0.05$, $n = 8$). Salinity and temperature may influence the vertical mixing of plastic particles.[44,63] The salinity of our study region was on average 36.07 ± 0.43 PSU (deployment#1) and 36.18 ± 0.37 PSU (deployment#2), with no significant differences between the

https://doi.org/10.1021/acs.est.2c04712
Environ. Sci. Technol. XXXX, XXX, XXX−XXX

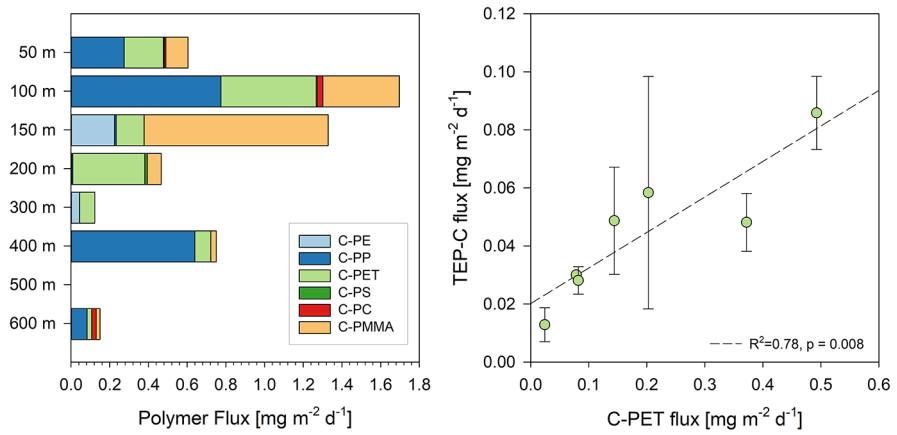

Figure 3. Left: Fluxes of the different clustered plastic polymer types observed in deployment#2. Samples have been PIT-control-blank corrected (cf. Materials and Methods) and only polymer clusters with positive values after PIT-control-blank correction are shown. Right: Linear regression between the fluxes of TEP-C and *C*-PET mass (PIT-control-blank corrected) in deployment#2.

two areas. Similarly, temperature ranged from 21.75 (50 m depth) to 10.48 °C (600 m) (deployment#1) and 20.79 (50 m depth) to 11.8 °C (600 m) (deployment#2) and no differences were found between deployment#1 and deployment#2.

The vertical export flux of plastic mass by Py-GC/MS significantly correlated to marine gel particles, that is, TEP and CSP and to a lesser extent to POC and PN (Figure 2). A strong correlation was evidenced in deployment#2 between *C*-PET and TEP (as particle number and carbon fluxes) (Figure 3). *C*-PET is a high-density polymer (1.33 g cm^{-3} on average) which would tend to sink in seawater, but it was encountered at any depth in this study. It accounted for about 27% of all plastic mass found by Py-GC/MS and was not influenced by significant ship or sampling device contamination (Figures 3, S3). No *C*-PET cluster was, however, evidenced by FT-IR analysis (Table S7). Given that only mass data were available (Py-GC/MS), a potential upper size threshold for *C*-PET was estimated by comparing the size of TEP particles in both deployments based on the ESD. The largest TEP particles had an ESD of 117 and 103 μm in deployment#1 and #2, respectively; it is therefore possible that *C*-PET comprised small microplastics ~120 μm or less in size.

In deployment#2, *C*-PET was the only cluster whose flux showed a significant positive correlation with salinity and temperature (Spearman r = 0.79, p = 0.015, n = 7 for both). Similarly, TEP fluxes were strongly positively dependent on these parameters (R^2 = 0.73, p = 0.007 for salinity, R^2 = 0.66, p = 0.014 for temperature). This suggests a general decrease of *C*-PET flux over depth, but it may also indicate that *C*-PET particle flux is highest when ambient seawater conditions are favorable for their biogenic components' carriers such as TEP. Fluxes from deployment#1 and deployment#2 were fitted to the power-law decrease model (Martin Curve) to estimate the attenuation coefficients b:[52] more negative b values indicate higher flux attenuation linked to faster degradation of biogenic components or a slowed sinking rate (Table S8). In both deployments, chlorophyll *a* had the highest flux attenuation being a more labile component compared to POC, PN, and marine gels (TEP, CSP), the latter being the faster sinking components among biogenic parameters (Table S8). Fluxes of plastic mass as determined by Py-GC/MS and extrapolated from FT-IR analysis decreased over depth but could not be fitted to the model[52] (p > 0.05, Table S8). From Py-GC/MS analysis in deployment#2, *C*-PET was the one cluster with the closest fitting of the export curve with a b value similar to POC and PN and higher than TEP and CSP. This suggests a strong dependency of *C*-PET export on the interaction with biogenic aggregates in our study area. Transfer efficiencies (T_{eff}, %) as the flux ratio 600 m/100 m (and 500 m/50 m for FT-IR) were calculated (Table S8): of the biogenic components, chlorophyll *a* had the lowest T_{eff} in both deployments, whereas TEP and CSP were the most efficiently exported. *C*-PP had a quite high T_{eff} in deployment#2 compared to other components (11%, Table S8), meaning that there must have been some *in situ* processes that favored the sinking of this polymer type. *C*-PP was the most abundant polymer cluster found and at almost any depth (Table 1). Highest T_{eff} were observed for FT-IR plastic mass in both deployments (Table S8).

To estimate a theoretical removal time of plastic from the surface and a possible settling velocity in our study area (deployment#2), we used *C*-PET as a model polymer cluster given its strong relation with TEP. Because Py-GC/MS cannot distinguish particle sizes, we considered three sizes: 10 μm ESD particle as the smallest (stainless-steel mesh for Py-GC/MS analysis), 55 and 103 μm ESD particles as the medium and largest (as the average and largest TEP−ESD found in deployment#2). We applied the average density of *C*-PET of 1.33 g cm^{-3} to the particles (Table 1) and assumed 'Stokes' equation for settling particles[45] (Materials and Methods).

The sinking rate for these particles' sizes ranged from 1.7 × 10^{-5} (~10 μm ESD) to 5 × 10^{-4} (~55 μm ESD) to 1.8 × 10^{-3} m s^{-1} (~103 μm ESD), corresponding to exports of 1.4, 43.4, and 152 meters per day, respectively.

Measured sinking velocities in the laboratory report comparable values between 2.6 ± 0.3 × 10^{-3} and 17 ± 0.7 × 10^{-3} m s^{-1} for virgin particles of various shapes in the range of 500−2000 μm diameter, at similar salinities.[64] Likewise, Kooi et al.[44] modeled that particles ~100 μm in diameter would sink about 100 m day^{-1} (1.16 × 10^{-3} m s^{-1}) in ocean conditions by assuming spherical particles and evenly distributed biofilm.

Based on these theoretical sinking velocities, small microplastics of this study (~10 μm ESD) would need over a year to reach depths of 600 m or more, and about 35 days to reach 50 m depth. Likewise, medium size and larger particles (~55 and ~103 μm ESD) would sink to 600 m or greater depths within 14 to 4 days, respectively, or to 150 m within 3.5 and 1 day. As previously noted, low transfer efficiencies can indicate that the particles sink slowly or are degraded fast. High transfer

https://doi.org/10.1021/acs.est.2c04712
Environ. Sci. Technol. XXXX, XXX, XXX−XXX

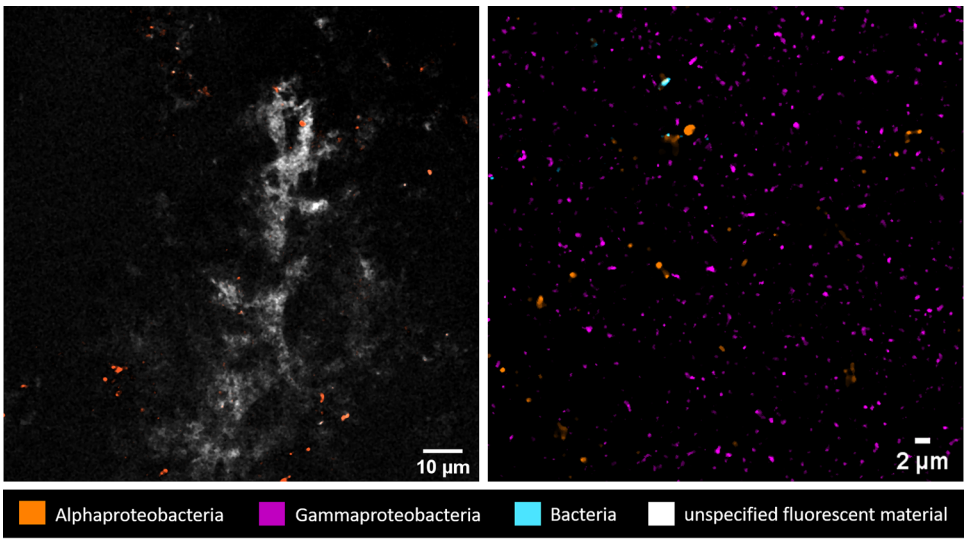

Figure 4. Biofilm communities on a plastic fragment (possibly a polyethylene or polypropylene particle) collected at 300 m within a sediment trap of deployment #1. The black background is the surface of the fragment. Patches of single cells belonging to the families *Alphaproteobacteria* (in orange) and *Gammaproteobacteria* (in pink) occurring occasionally on the particle surface. However, most of the surface is unsettled or covered with unidentified sticky material (perhaps biofilm extracellular exopolymer substances, EPS) that is embedding or is surrounded by single bacteria cells.

efficiencies instead could be due to fast sinking or little degradation. The largest TEP particle found at 600 m in deployment#2 had an ESD of 69 μm and a *C*-PET particle of this size, in our study area, would need about 9 days to reach that depth. By looking at the transfer efficiencies of plastic mass (Py-GC/MS) and TEP, we can imagine that aggregation with biogenic material likely enhances sinking velocities. TEP are known to be the glue that favors marine snow formation,[65] thus it is likely that plastics aggregate with TEP and other sinking particles forming rapidly settling marine snow. We collected single plastic debris of 1 mm at 300 m depth and investigated its biofilm composition using a confocal laser scanning microscope technique called combinatorial labeling and spectral imaging-fluorescence *in situ* hybridization (CLASI-FISH).[61] The debris was covered with small patches of bacteria clusters mainly composed of *Alpha-* and *Gammaproteobacteria* (Figure 4), two common classes usually found on plastic debris in the surface oceans.[66] Bacteria are attached randomly as single cells to the debris surface, or they are embedded in gel-like structures. The presence of EPS excreted for attachment purposes and of a biofilm can also exert a microbial protective function against sudden external changes,[21] such as the high salinity of the brine where the debris was trapped. Such salinity gradient might have slowed down microbial activity (which was not assessed in our study) and for the same reason, we do not expect significant degradation processes occurring on marine snow particles during the settling time into the traps. Rather, the interaction of low-density plastic with marine aggregates and marine gels allowed even low-density plastics to be trapped into the brine solution. The fact that the main part of the plastic debris found at 300 m was biofilm-free might refer to an effective remineralization process in the deep independently from the sampling approach and/or a reduced biomass production.

DISCUSSION

The mismatch between the estimated plastic entering the ocean through rivers and the amount of plastic detected at the ocean's surface initially led the scientific community to suggest that there is a high percentage of "missing plastic" in marine environments.[41,42] More recently, Weiss and colleagues[67] have shown that most previous studies were based on an overestimation of river fluxes due to data scarcity, and through their new calculations, the authors proposed that the estimated plastic residence time at the ocean's surface increases from what was previously thought. Nevertheless, selective sequestration of small microplastics through various mechanisms occurs in the ocean and yet, the plastic cycling and transfer processes from the surface to the deep ocean are not fully understood, highlighting the need of reliable measures of plastic fluxes.[67]

Repeated episodes of fouling, sinking, defouling, and resurfacing further complicate our understanding of plastic particles' dynamics.[68] Low-density polymers represent over 65.5% of the global plastic production and in principle they would have positive buoyancy at sea.[69] A comparison of modeling approaches from the literature,[15,41,70] partly based on monitored data, emphasized that only about 1% of the theoretically introduced plastics into the marine environment are recovered as floating plastics.[71] This suggests mechanisms yet unexplored driving plastic fate in marine environments. Microplastics can travel throughout the water column by being ingested or embedded into fecal pellets; however, there might be other processes vectoring plastics to the ocean sediments,[72] of unknown speed. Plastic particles' movements within the water column are mostly derived from modeling approaches,[40,44,73,74] and observations of plastics at intermediate and greater depths are more scarce.[37,45,75] Plastic littering has severe ecological implications and impacts on different species populating different depths.[45,75] Quantifying plastic fluxes to the deep sea is fundamental to understand plastic removal dynamics from the surface, the potential risks to marine biota, as well as plastic interaction with biogeochemical cycles and microbial communities that can affect global ecosystem's food webs, nutrient availability, carbon dynamics, with potential repercussion on carbon storage and the biological carbon pump of a changing ocean.[32] *In situ* conditions such as salinity, temperature, chlorophyll, and the amount of dissolved and particulate organic compounds, as well as polymer characteristics, may influence plastic residence times in the water column: knowing plastic

https://doi.org/10.1021/acs.est.2c04712
Environ. Sci. Technol. XXXX, XXX, XXX−XXX

transfer into (sources) and within the environment, accumulation patterns and interaction with biotic and abiotic compartments is a requirement to develop global prevention and mitigation strategies.

In this study, we captured plastic particles' downward fluxes down to 600 m depth, with a complementary approach to deep ocean sampling techniques such as high-volume *in situ* pumps, ROVs, or CTD casts. The deployment of sediment traps proved as a good method to study how the plastic export in the ocean depends on biological activity and biogenic compounds' fluxes, while providing an estimated removal time of microplastics from the water column. Additionally, plastic embedded in aggregates or as single debris can gently be collected in deep ocean sediment traps by keeping fragile biofilm structures intact. Longer sampling times of days to weeks enhance the chance to gather a reasonable amount of debris for microbial community studies. The one plastic fragment that was collected at 300 m depth revealed small areas of bacterial colonization on the surface as well as a polysaccharidic structure related to EPS; EPS is released by microbial cells to facilitate attachment, is the foundation of the biofilm structure on plastic debris,[21] and as marine gels, is an important constituent of marine snow.[29] The plastisphere microbes might be a selected community still adapting to colonize these new environmental niches, and studies have shown a richness of species changing over time, with diatoms as early colonizers in the sunlit ocean, followed by *Gammaproteobacteria* and *Alphaproteobacteria* as the community becomes more mature,[21] as found in our sample. *Rhodobacteraceae* (*Alphaproteobacteria*) are a dominant taxon on plastic and ubiquitously present at all stages of biofilm development because the EPS they release helps the settlement of other microbial organisms.[21] These taxa are also found in seawater, but *Gammaproteobacteria*, for example, are important colonizers of marine snow particles as well.[22] As pointed out, the fact that only a few patches with a biofilm-like structure were individuated on the plastic fragment suggests a higher remineralization of organic material at depth, where the interaction of plastics with biogenic sinking material further concentrates microbial activity in these agglomerates as "nutrient hot spots" in oligotrophic regions.

Our study suggests that export fluxes of plastic in marine systems are dependent on particles' size and that plastics between 10 and ∼100 μm are most likely entrapped into biogenic aggregates, a process that determines these plastics' removal from the water along with the flux attenuation of marine snow,[52] whereas larger particles may follow different dynamics. According to our estimated removal rates, the sinking of microplastics (<100 μm) from the surface would need longer times unless they are incorporated into organic matrices that carry these particles down to the deep ocean. This might be particularly true for polymers that have a lower density than seawater (C-PP in our study). The highest amount of plastic mass we detected in fact was found between 100 and 150 m depth, which coincided with high concentrations of chlorophyll *a*, marine gel particles, and particulate organic components in general; based on our estimates, particles of larger diameters (and hence, larger mass) sank faster when interacting with marine snow aggregates, explaining the lower plastic mass and residence time in the upper 50 m of the water column. Recent observations for the South Atlantic Gyre report an even distribution of particles in the water column and theoretical slow sinking velocities for microplastics (10−300 μm) apparently not influenced by density gradients.[45] There is thus a large amount of microplastics (<1000 μm) that we can trace down to the deep sea, which may range from ∼240 particles m^{-3}[45] to a median number between ∼200 and ∼800 particles m^{-3} as found here by FT-IR analysis (Table S6) or even much higher if smaller particles are considered. The interaction of smaller plastic particles (∼100 μm) with biogenic components such as TEP and CSP may determine vertical plastic hot spots and bioavailability in this size range for animal feeding. Particles embedded into marine snow are likely to attract planktonic species and larger animals. High plastic particles' abundance would increase the probability of encounter and the ecological risks for marine organisms. Moreover, micro- and nanoplastics play a so far neglected role in marine biogeochemical cycling as a modern anthropogenic and long-lasting seawater compound, and a new component of the marine carbon cycle.[4,32] Field evidences point to high incorporation of plastics in marine aggregates in coastal seas, and that the smaller sized aggregates containing plastic (∼50 to 400 μm) are frequently ingested, for example, by common blue mussels (*Mytilus edulis*)[26]. *Mytilus* ssp. are found in intertidal and coastal areas worldwide in temperate to polar waters.[76] At least 13 zooplankton taxa can ingest PS particles between 7 and 30 μm, and ingestion of 7 μm microplastics may decrease algal feeding.[77] When zooplankton preferentially grazes on plastic, it reduces the pressure on primary producers; in areas of enough nutrient concentrations, this phenomenon accelerates biological production and subsequent degradation and oxygen loss.[24] In oxygen-deficient areas, the transfer efficiency of organic matter is higher than in well-oxygenated waters.[46] In these regions, we may expect that a higher flux of particulate organics (e.g., TEP) will also affect the dynamics of plastic particles reaching the deep ocean.

Plastic contains about 80% carbon by weight, and as a colonization surface, it can attract more biologically produced carbon.[20] The knowledge of fluxes helps understanding plastic impact on carbon and nutrient cycling, an important parameter for present and future changes in the marine biological carbon pump and in the ocean's capacity to mitigate climate change.[32] In our results, the flux of plastic-C reaching the deep sea was as high as 3.8% of the POC flux and even exceeded the flux of the carbon share contained in individual biogenic components (TEP). We suggest that the plastic-C may also partly explain the molecularly uncharacterized fraction of sinking POC below the euphotic zone, so far proposed being lipid-like material, highly aliphatic molecules sorbed to old dissolved organic carbon from the water column or suspended POC based on its $\Delta^{14}C$ and $\delta^{13}C$ signatures.[78] Today sinking plastic-C may represent a significant amount of the marine carbon pump. As the total oceanic carbon flux has a large anthropogenic component to be considered, the paradigm of natural cycling of elements probably needs to be revised.

Our field observations show that the transfer efficiency and the vertical flux attenuation of marine gels and plastic mass is tightly related, and these components might mutually influence each other's export in the water column according to models suggesting a "biological plastic sink".[40] Whether plastic accelerates or slows down the export of carbon as marine snow and marine gels is difficult to say, as it would need a comparison to a "zero plastic" field scenario. On the other end, marine snow can act as a purging mechanism channeling plastic from the surface to marine sediments, where plastics accumulation hot spots at the seafloor may significantly impact benthic ecology and community activities with physical (by the plastic itself) and chemical effects (via leachates and contaminants adsorbed on the plastic's surface) on mortality,

https://doi.org/10.1021/acs.est.2c04712
Environ. Sci. Technol. XXXX, XXX, XXX−XXX

reproduction, development, and increased oxygen consumption.[79]

Further efforts could aim at determining a microplastic size threshold that can significantly stimulate a local carbon production through biofilm biomass. Our study highlights that marine biogenic polymers may embed a large number of small plastics, and these aggregates drive plastic export to the deep ocean, plastic interaction with biota, and plastic "diffusion" into the marine carbon cycle. These empirical data might be useful to study plastic effects on marine food webs and carbon cycling in different marine compartments, and they highlight the urgency of actions to prevent plastic from entering marine environments.

■ ASSOCIATED CONTENT

Supporting Information

The Supporting Information is available free of charge at https://pubs.acs.org/doi/10.1021/acs.est.2c04712.

Additional experimental details, methods, and results with photos, graphs, and tables supporting the main text (PDF)

■ AUTHOR INFORMATION

Corresponding Author

Luisa Galgani − *GEOMAR Helmholtz Center for Ocean Research Kiel, D-24105 Kiel, Germany; Harbor Branch Oceanographic Institute, Florida Atlantic University, Fort Pierce, Florida 34946, United States;* orcid.org/0000-0001-5239-6893; Email: lgalgani@geomar.de

Authors

Isabel Goßmann − *Institute for Chemistry and Biology of the Marine Environment (ICBM), Carl von Ossietzky University of Oldenburg, D-26111 Oldenburg, Germany*

Barbara Scholz-Böttcher − *Institute for Chemistry and Biology of the Marine Environment (ICBM), Carl von Ossietzky University of Oldenburg, D-26111 Oldenburg, Germany;* orcid.org/0000-0002-3287-4218

Xiangtao Jiang − *The University of Texas at Austin, Marine Science Institute, Port Aransas, Texas 78373, United States*

Zhanfei Liu − *The University of Texas at Austin, Marine Science Institute, Port Aransas, Texas 78373, United States;* orcid.org/0000-0002-8897-0698

Lindsay Scheidemann − *GEOMAR Helmholtz Center for Ocean Research Kiel, D-24105 Kiel, Germany*

Cathleen Schlundt − *GEOMAR Helmholtz Center for Ocean Research Kiel, D-24105 Kiel, Germany*

Anja Engel − *GEOMAR Helmholtz Center for Ocean Research Kiel, D-24105 Kiel, Germany*

Complete contact information is available at: https://pubs.acs.org/10.1021/acs.est.2c04712

Author Contributions

The manuscript was written through contributions of all authors. All authors have given approval to the final version of the manuscript. Conceptualization: A.E.; data collection, data analysis, manuscript writing: L.G.; sample analysis: A.E., B.S.B., I.G., C.S., X.J., Z.L., and L.S.; editing and review: L.G., A.E., B.S.B., I.G., C.S., X.J., Z.L., and L.S.

Funding

Helmholtz Association (GEOMAR) and the Bundesministerium für Bildung und Forschung, BMBF in the joint research project FACTS ID 03F0849B and 03F0849C, JPI-Oceans, for GEOMAR (AE, CS) and ICBM (IG, BSB); National Science Foundation #2033828, UTexas (ZL, XJ); and European Union's Horizon 2020 research and innovation programme under the Marie Sklodowska-Curie grant agreement No. 882682 (LG).

Notes

The authors declare no competing financial interest.

■ ACKNOWLEDGMENTS

We profoundly thank J. Roa for his assistance during the POS536 cruise from Azores to Malaga and in the lab, as well as M. Lenz as chief scientist and the whole ship and scientific crew of the expedition. A. Mutzberg is greatly acknowledged for taking care of CTD data as well as T. Klüver for lab analysis of POC, PN, and Chl *a*. We would also like to thank H. Niland for her assistance with FT-IR analyses.

■ ABBREVIATIONS

C-PA6	polyamide-6 cluster
C-PC	polycarbonate cluster
C-PE	polyethylene cluster
C-PET	polyethylene terephthalate cluster
C-MDI-PUR	methylene diphenyl diisocyanate polyurethane cluster
C-PMMA	polymethyl methacrylate cluster
C-PP	polypropylene cluster
C-PS	polystyrene cluster
C-PVC	polyvinylchloride cluster
Chl *a*	chlorophyll *a*
CSP	Coomassie stainable particles
CTD	conductivity, temperature, and depth
DOC	dissolved organic carbon
DOM	dissolved organic matter
EPS	extracellular polymeric substances
ESD	equivalent spherical diameter
FT-IR	Fourier transform infrared
GPS	global positioning system
LDPE	low-density polyethylene
MCT	mercury cadmium telluride (detector)
MT	million metric tons
PIT	particle interceptor trap
plastic-C	carbon contained in plastic
PN	particulate nitrogen
POC	particulate organic carbon
POM	particulate organic matter
Py-GC/MS	pyrolysis gas chromatography coupled with mass spectrometry
ROV	remote operated vehicle
TEP	transparent exopolymer particles
TEP-C	carbon contained in TEP particles
T_{eff}	transfer efficiencies (%)
TPM	total particulate mass

■ REFERENCES

(1) Ross, P. S.; Chastain, S.; Vassilenko, E.; Etemadifar, A.; Zimmermann, S.; Quesnel, S. A.; Eert, J.; Solomon, E.; Patankar, S.; Posacka, A. M.; Williams, B. Pervasive distribution of polyester fibres in the Arctic Ocean is driven by Atlantic inputs. *Nat. Commun.* **2021**, *12*, 106.

(2) Cózar, A.; Martí, E.; Duarte, C. M.; García-de-Lomas, J.; van Sebille, E.; Ballatore, T. J.; Eguíluz, V. M.; González-Gordillo, J. I.; Pedrotti, M. L.; Echevarría, F.; Troublè, R.; Irigoien, X. The Arctic Ocean as a dead end for floating plastics in the North Atlantic branch of the Thermohaline Circulation. *Sci. Adv.* **2017**, *3*, No. e1600582.

(3) Kelly, A.; Lannuzel, D.; Rodemann, T.; Meiners, K. M.; Auman, H. J. Microplastic contamination in east Antarctic sea ice. *Mar. Pollut. Bull.* **2020**, *154*, 111130.
(4) Stubbins, A.; Law, K. L.; Muñoz, S. E.; Bianchi, T. S.; Zhu, L. Plastics in the Earth system. *Science* **2021**, *373*, 51−55.
(5) Bergmann, M.; Mützel, S.; Primpke, S.; Tekman, M. B.; Trachsel, J.; Gerdts, G. White and wonderful? Microplastics prevail in snow from the Alps to the Arctic. *Sci. Adv.* **2019**, *5*, No. eaax1157.
(6) Wright, S. L.; Ulke, J.; Font, A.; Chan, K. L. A.; Kelly, F. J. Atmospheric microplastic deposition in an urban environment and an evaluation of transport. *Environ. Int.* **2020**, *136*, 105411.
(7) Villarrubia-Gómez, P.; Cornell, S. E.; Fabres, J. Marine plastic pollution as a planetary boundary threat - The drifting piece in the sustainability puzzle. *Mar. Pol.* **2018**, *96*, 213−220.
(8) Gunthe, S. S.; Liu, P.; Panda, U.; Raj, S. S.; Sharma, A.; Darbyshire, E.; Reyes-Villegas, E.; Allan, J.; Chen, Y.; Wang, X.; Song, S.; Pöhlker, M. L.; Shi, L.; Wang, Y.; Kommula, S. M.; Liu, T.; Ravikrishna, R.; McFiggans, G.; Mickley, L. J.; Martin, S. T.; Pöschl, U.; Andreae, M. O.; Coe, H. Enhanced aerosol particle growth sustained by high continental chlorine emission in India. *Nat. Geosci.* **2021**, *14*, 77−84.
(9) Schmidt, C.; Krauth, T.; Wagner, S. Export of Plastic Debris by Rivers into the Sea. *Environ. Sci. Technol.* **2017**, *51*, 12246−12253.
(10) Meijer, L. J. J.; van Emmerik, T. v.; van der Ent, R. v. d.; Schmidt, C.; Lebreton, L. More than 1000 rivers account for 80% of global riverine plastic emissions into the ocean. *Sci. Adv.* **2021**, *7*, No. eaaz5803.
(11) Dibke, C.; Fischer, M.; Scholz-Böttcher, B. M. Microplastic Mass Concentrations and Distribution in German Bight Waters by Pyrolysis-Gas Chromatography-Mass Spectrometry/Thermochemolysis Reveal Potential Impact of Marine Coatings: Do Ships Leave Skid Marks? *Environ. Sci. Technol.* **2021**, *55*, 2285−2295.
(12) Leistenschneider, C.; Burkhardt-Holm, P.; Mani, T.; Primpke, S.; Taubner, H.; Gerdts, G. Microplastics in the Weddell Sea (Antarctica): A Forensic Approach for Discrimination between Environmental and Vessel-Induced Microplastics. *Environ. Sci. Technol.* **2021**, *55*, 15900−15911.
(13) Turner, A. Paint particles in the marine environment: An overlooked component of microplastics. *Water Res.: X* **2021**, *12*, 100110.
(14) Bank, M. S.; Hansson, S. V. The Plastic Cycle: A Novel and Holistic Paradigm for the Anthropocene. *Environ. Sci. Technol.* **2019**, *53*, 7177−7179.
(15) Jambeck, J. R.; Geyer, R.; Wilcox, C.; Siegler, T. R.; Perryman, M.; Andrady, A.; Narayan, R.; Law, K. L. Plastic waste inputs from land into the ocean. *Science* **2015**, *347*, 768−771.
(16) Falkowski, P.; Scholes, R. J.; Boyle, E.; Canadell, J.; Canfield, D.; Elser, J.; Gruber, N.; Hibbard, K.; Högberg, P.; Linder, S.; Mackenzie, F. T.; Moore III, B., 3rd; Pedersen, T.; Rosenthal, Y.; Seitzinger, S.; Smetacek, V.; Steffen, W. The Global Carbon Cycle: A Test of Our Knowledge of Earth as a System. *Science* **2000**, *290*, 291−296.
(17) Romera-Castillo, C.; Pinto, M.; Langer, T. M.; Álvarez-Salgado, X. A.; Herndl, G. J. Dissolved organic carbon leaching from plastics stimulates microbial activity in the ocean. *Nat. Commun.* **2018**, *9*, 1430.
(18) Galgani, L.; Engel, A.; Rossi, C.; Donati, A.; Loiselle, S. A. Polystyrene microplastics increase microbial release of marine Chromophoric Dissolved Organic Matter in microcosm experiments. *Sci. Rep.* **2018**, *8*, 14635.
(19) Galgani, L.; Loiselle, S. A. Plastic Accumulation in the Sea Surface Microlayer: An Experiment-Based Perspective for Future Studies. *Geosciences* **2019**, *9*, 66.
(20) Galgani, L.; Tsapakis, M.; Pitta, P.; Tsiola, A.; Tzempelikou, E.; Kalantzi, I.; Esposito, C.; Loiselle, A.; Tsotskou, A.; Zivanovic, S.; Dafnomili, E.; Diliberto, S.; Mylona, K.; Magiopoulos, I.; Zeri, C.; Pitta, E.; Loiselle, S. A. Microplastics increase the marine production of particulate forms of organic matter. *Environ. Res. Lett.* **2019**, *14*, 124085.
(21) Amaral-Zettler, L. A.; Zettler, E. R.; Mincer, T. J. Ecology of the plastisphere. *Nat. Rev. Microbiol.* **2020**, *18*, 139−151.
(22) DeLong, E. F.; Franks, D. G.; Alldredge, A. L. Phylogenetic diversity of aggregate-attached vs. free-living marine bacterial assemblages. *Limnol. Oceanogr.* **1993**, *38*, 924−934.
(23) Rogers, K. L.; Carreres-Calabuig, J. A.; Gorokhova, E.; Posth, N. R. Micro-by-micro interactions: How microorganisms influence the fate of marine microplastics. *Limnol. Oceanogr. Lett.* **2020**, *5*, 18−36.
(24) Kvale, K.; Prowe, A. E. F.; Chien, C. T.; Landolfi, A.; Oschlies, A. Zooplankton grazing of microplastic can accelerate global loss of ocean oxygen. *Nat. Commun.* **2021**, *12*, 2358.
(25) Summers, S.; Henry, T.; Gutierrez, T. Agglomeration of nano- and microplastic particles in seawater by autochthonous and de novo-produced sources of exopolymeric substances. *Mar. Pollut. Bull.* **2018**, *130*, 258−267.
(26) Zhao, S.; Ward, J. E.; Danley, M.; Mincer, T. J. Field-Based Evidence for Microplastic in Marine Aggregates and Mussels: Implications for Trophic Transfer. *Environ. Sci. Technol.* **2018**, *52*, 11038−11048.
(27) Michels, J.; Stippkugel, A.; Lenz, M.; Wirtz, K.; Engel, A. Rapid aggregation of biofilm-covered microplastics with marine biogenic particles. *Proc. R. Soc. B* **1885**, *285*, 20181203.
(28) Engel, A.; Endres, S.; Galgani, L.; Schartau, M. Marvelous Marine Microgels: On the Distribution and Impact of Gel-Like Particles in the Oceanic Water-Column. *Front. Mar. Sci.* **2020**, *7*, 405.
(29) Decho, A. W.; Gutierrez, T. Microbial Extracellular Polymeric Substances (EPSs) in Ocean Systems. *Front. Microbiol.* **2017**, *8*, 922.
(30) Galloway, T. S.; Cole, M.; Lewis, C. Interactions of microplastic debris throughout the marine ecosystem. *Nat. Ecol. Evol.* **2017**, *1*, 0116.
(31) Jiao, N.; Herndl, G. J.; Hansell, D. A.; Benner, R.; Kattner, G.; Wilhelm, S. W.; Kirchman, D. L.; Weinbauer, M. G.; Luo, T.; Chen, F.; Azam, F. Microbial production of recalcitrant dissolved organic matter: long-term carbon storage in the global ocean. *Nat. Rev. Microbiol.* **2010**, *8*, 593−599.
(32) Galgani, L.; Loiselle, S. A. Plastic pollution impacts on marine carbon biogeochemistry. *Environ. Pollut.* **2021**, *268*, 115598.
(33) Shen, M.; Ye, S.; Zeng, G.; Zhang, Y.; Xing, L.; Tang, W.; Wen, X.; Liu, S. Can microplastics pose a threat to ocean carbon sequestration? *Mar. Pollut. Bull.* **2020**, *150*, 110712.
(34) Law, K. L.; Morét-Ferguson, S.; Maximenko, N. A.; Proskurowski, G.; Peacock, E. E.; Hafner, J.; Reddy, C. M. Plastic Accumulation in the North Atlantic Subtropical Gyre. *Science* **2010**, *329*, 1185−1188.
(35) Carpenter, E. J.; Smith, K. L. Plastics on the Sargasso Sea Surface. *Science* **1972**, *175*, 1240−1241.
(36) Ostle, C.; Thompson, R. C.; Broughton, D.; Gregory, L.; Wootton, M.; Johns, D. G. The rise in ocean plastics evidenced from a 60-year time series. *Nat. Commun.* **2019**, *10*, 1622.
(37) Pabortsava, K.; Lampitt, R. S. High concentrations of plastic hidden beneath the surface of the Atlantic Ocean. *Nat. Commun.* **2020**, *11*, 4073.
(38) Courtene-Jones, W.; Quinn, B.; Ewins, C.; Gary, S. F.; Narayanaswamy, B. E. Consistent microplastic ingestion by deep-sea invertebrates over the last four decades (1976-2015), a study from the North East Atlantic. *Environ. Pollut.* **2019**, *244*, 503−512.
(39) Courtene-Jones, W.; Quinn, B.; Ewins, C.; Gary, S. F.; Narayanaswamy, B. E. Microplastic accumulation in deep-sea sediments from the Rockall Trough. *Mar. Pollut. Bull.* **2020**, *154*, 111092.
(40) Kvale, K.; Prowe, A. E. F.; Chien, C. T.; Landolfi, A.; Oschlies, A. The global biological microplastic particle sink. *Sci. Rep.* **2020**, *10*, 16670.
(41) Cózar, A.; Echevarría, F.; González-Gordillo, J. I.; Irigoien, X.; Úbeda, B.; Hernández-León, S.; Palma, A. T.; Navarro, S.; García-de-Lomas, J.; Ruiz, A.; Fernández-de-Puelles, M. L.; Duarte, C. M. Plastic debris in the open ocean. *Proc. Natl. Acad. Sci. U.S.A.* **2014**, *111*, 10239−10244.
(42) Mintenig, S. M.; Bäuerlein, P. S.; Koelmans, A. A.; Dekker, S. C.; van Wezel, A. P. Closing the gap between small and smaller: towards a framework to analyse nano- and microplastics in aqueous environmental samples. *Environ. Sci.: Nano* **2018**, *5*, 1640−1649.

https://doi.org/10.1021/acs.est.2c04712
Environ. Sci. Technol. XXXX, XXX, XXX−XXX

(43) Thompson, R. C.; Olsen, Y.; Mitchell, R. P.; Davis, A.; Rowland, S. J.; John, A. W.; McGonigle, D.; Russell, A. E. Lost at sea: where is all the plastic? *Science* **2004**, *304*, 838.
(44) Kooi, M.; Nes, E. H. v.; Scheffer, M.; Koelmans, A. A. Ups and Downs in the Ocean: Effects of Biofouling on Vertical Transport of Microplastics. *Environ. Sci. Technol.* **2017**, *51*, 7963−7971.
(45) Zhao, S.; Zettler, E. R.; Bos, R. P.; Lin, P.; Amaral-Zettler, L. A.; Mincer, T. J. Large quantities of small microplastics permeate the surface ocean to abyssal depths in the South Atlantic Gyre. *Global Change Biol.* **2022**, *28*, 2991−3006.
(46) Engel, A.; Wagner, H.; Le Moigne, F. A. C.; Wilson, S. T. Particle export fluxes to the oxygen minimum zone of the eastern tropical North Atlantic. *Biogeosciences* **2017**, *14*, 1825−1838.
(47) Buesseler, K. O.; Antia, A. N.; Chen, M.; Fowler, S. W.; Gardner, W. D.; Gustafsson, Ö.; Harada, K.; Michaels, A. F.; Rutgers van der Loeff, M.; Sarin, M.; Steinberg, D. K.; Trull, T. An assessment of the use of sediment traps for estimating upper ocean particle fluxes. *J. Mar. Res.* **2007**, *65*, 345−416.
(48) Knauer, G. A.; Martin, J. H.; Bruland, K. W. Fluxes of particulate carbon, nitrogen, and phosphorus in the upper water column of the northeast Pacific. *Deep-Sea Res. Part A Oceanogr. Res. Pap.* **1979**, *26*, 97−108.
(49) Estapa, M.; Valdes, J.; Tradd, K.; Sugar, J.; Omand, M.; Buesseler, K. The Neutrally Buoyant Sediment Trap: Two Decades of Progress. *J. Atmos. Ocean. Technol.* **2020**, *37*, 957−973.
(50) Soutar, A.; Kling, S. A.; Crill, P. A.; Duffrin, E.; Bruland, K. W. Monitoring the marine environment through sedimentation. *Nature* **1977**, *266*, 136−139.
(51) Le Moigne, F. A. C.; Cisternas-Novoa, C.; Piontek, J.; Maßmig, M.; Engel, A. On the effect of low oxygen concentrations on bacterial degradation of sinking particles. *Sci. Rep.* **2017**, *7*, 16722.
(52) Martin, J. H.; Knauer, G. A.; Karl, D. M.; Broenkow, W. W. VERTEX: carbon cycling in the northeast Pacific. *Deep-Sea Res. Part A Oceanogr. Res. Pap.* **1987**, *34*, 267−285.
(53) Welschmeyer, N. A. Fluorometric analysis of chlorophyll a in the presence of chlorophyll b and pheopigments. *Limnol. Oceanogr.* **1994**, *39*, 1985−1992.
(54) Engel, A. Determination of Marine Gel Particles. In *Practical Guidelines for the Analysis of Seawater*, 1st ed.; Wurl, O., Ed.; CRC Press, 2009, Chapter 7ISBN: 978-1-420-07306-5. 10.1201/9781420073072.
(55) Mari, X. Carbon content and C:N ratio of transparent exopolymeric particles (TEP) produced by bubbling exudates of diatoms. *Mar. Ecol.: Prog. Ser.* **1999**, *183*, 59−71.
(56) Fischer, M.; Scholz-Böttcher, B. M. Microplastics analysis in environmental samples—recent pyrolysis-gas chromatography-mass spectrometry method improvements to increase the reliability of mass-related data. *Anal. Methods* **2019**, *11*, 2489−2497.
(57) Goßmann, I.; Halbach, M.; Scholz-Böttcher, B. M. Car and truck tire wear particles in complex environmental samples—A quantitative comparison with "traditional" microplastic polymer mass loads. *Sci. Total Environ.* **2021**, *773*, 145667.
(58) Primpke, S.; Fischer, M.; Lorenz, C.; Gerdts, G.; Scholz-Böttcher, B. M. Comparison of pyrolysis gas chromatography/mass spectrometry and hyperspectral FTIR imaging spectroscopy for the analysis of microplastics. *Anal. Bioanal. Chem.* **2020**, *412*, 8283−8298.
(59) Cole, M.; Webb, H.; Lindeque, P. K.; Fileman, E. S.; Halsband, C.; Galloway, T. S. Isolation of microplastics in biota-rich seawater samples and marine organisms. *Sci. Rep.* **2014**, *4*, 4528.
(60) Di, M.; Wang, J. Microplastics in surface waters and sediments of the Three Gorges Reservoir, China. *Sci. Total Environ.* **2018**, *616−617*, 1620−1627.
(61) Schlundt, C.; Mark Welch, J. L.; Knochel, A. M.; Zettler, E. R.; Amaral-Zettler, L. A. Spatial structure in the "Plastisphere": Molecular resources for imaging microscopic communities on plastic marine debris. *Mol. Ecol. Resour.* **2020**, *20*, 620−634.
(62) Ardekani, A. M.; Stocker, R. S. Stratlets: Low Reynolds Number Point-Force Solutions in a Stratified Fluid. *Phys. Rev. Lett.* **2010**, *105*, 084502.
(63) Kukulka, T.; Law, K. L.; Proskurowski, G. Evidence for the Influence of Surface Heat Fluxes on Turbulent Mixing of Microplastic Marine Debris. *J. Phys. Oceanogr.* **2016**, *46*, 809−815.
(64) Kowalski, N.; Reichardt, A. M.; Waniek, J. J. Sinking rates of microplastics and potential implications of their alteration by physical, biological, and chemical factors. *Mar. Pollut. Bull.* **2016**, *109*, 310−319.
(65) Passow, U.; Alldredge, A. L.; Logan, B. E. The role of particulate carbohydrate exudates in the flocculation of diatom blooms. *Deep-Sea Res. Part I Oceanogr. Res. Pap.* **1994**, *41*, 335−357.
(66) De Tender, C.; Schlundt, C.; Devriese, L. I.; Mincer, T. J.; Zettler, E. R.; Amaral-Zettler, L. A. A review of microscopy and comparative molecular-based methods to characterize "Plastisphere" communities. *Anal. Methods* **2017**, *9*, 2132−2143.
(67) Weiss, L.; Ludwig, W.; Heussner, S.; Canals, M.; Ghiglione, J.-F.; Estournel, C.; Constant, M.; Kerhervé, P. The missing ocean plastic sink: Gone with the rivers. *Science* **2021**, *373*, 107−111.
(68) Lebreton, L.; Egger, M.; Slat, B. A global mass budget for positively buoyant macroplastic debris in the ocean. *Sci. Rep.* **2019**, *9*, 12922.
(69) Geyer, R.; Jambeck, J. R.; Law, K. L. Production, use, and fate of all plastics ever made. *Sci. Adv.* **2017**, *3*, No. e1700782.
(70) Eriksen, M.; Lebreton, L. C.; Carson, H. S.; Thiel, M.; Moore, C. J.; Borerro, J. C.; Galgani, F.; Ryan, P. G.; Reisser, J. Plastic Pollution in the World's Oceans: More than 5 Trillion Plastic Pieces Weighing over 250,000 Tons Afloat at Sea. *PLoS One* **2014**, *9*, No. e111913.
(71) Oberbeckmann, S.; Labrenz, M. Marine Microbial Assemblages on Microplastics: Diversity, Adaptation, and Role in Degradation. *Ann. Rev. Mar. Sci.* **2020**, *12*, 209−232.
(72) Angiolillo, M. Debris in Deep Water. In *World Seas: An Environmental Evaluation*, 2nd ed.; Sheppard, C., Ed.; Academic Press, 2019; pp 251−268, Chapter 14ISBN: 9780128050521. 10.1016/B978-0-12-805052-1.00015-2.
(73) Koelmans, A. A.; Kooi, M.; Law, K. L.; van Sebille, E. All is not lost: deriving a top-down mass budget of plastic at sea. *Environ. Res. Lett.* **2017**, *12*, 114028.
(74) Kooi, M.; Reisser, J.; Slat, B.; Ferrari, F. F.; Schmid, M. S.; Cunsolo, S.; Brambini, R.; Noble, K.; Sirks, L. A.; Linders, T. E.; Schoeneich-Argent, R. I.; Koelmans, A. A. The effect of particle properties on the depth profile of buoyant plastics in the ocean. *Sci. Rep.* **2016**, *6*, 33882.
(75) Choy, C. A.; Robison, B. H.; Gagne, T. O.; Erwin, B.; Firl, E.; Halden, R. U.; Hamilton, J. A.; Katija, K.; Lisin, S. E.; Rolsky, C.; Van Houtan, K. The vertical distribution and biological transport of marine microplastics across the epipelagic and mesopelagic water column. *Sci. Rep.* **2019**, *9*, 7843.
(76) Mathiesen, S. S.; Thyrring, J.; Hemmer-Hansen, J.; Berge, J.; Sukhotin, A.; Leopold, P.; Bekaert, M.; Sejr, M. K.; Nielsen, E. E. Genetic diversity and connectivity withinMytilusspp. in the subarctic and Arctic. *Evol. Appl.* **2016**, *10*, 39−55.
(77) Cole, M.; Lindeque, P.; Fileman, E.; Halsband, C.; Goodhead, R.; Moger, J.; Galloway, T. S. Microplastic Ingestion by Zooplankton. *Environ. Sci. Technol.* **2013**, *47*, 6646−6655.
(78) Hwang, J.; Druffel, E. R. M. Lipid-Like Material as the Source of the Uncharacterized Organic Carbon in the Ocean? *Science* **2003**, *299*, 881−884.
(79) Haegerbaeumer, A.; Mueller, M.-T.; Fueser, H.; Traunspurger, W. Impacts of Micro- and Nano-Sized Plastic Particles on Benthic Invertebrates: A Literature Review and Gap Analysis. *Front. Environ. Sci.* **2019**, *7*, 17.

https://doi.org/10.1021/acs.est.2c04712
Environ. Sci. Technol. XXXX, XXX, XXX−XXX